ADVANCED MATERIALS INTERFACES
Open Access
www.advmatinterfaces.de

A Duality Between Surface Charge and Work Function in Scanning Kelvin Probe Microscopy

Isaac C.D. Lenton, Felix Pertl, Lubuna Shafeek, and Scott R. Waitukaitis*

Scanning Kelvin probe microscopy (SKPM) is a powerful technique for macroscopic imaging of the electrostatic potential above a surface. Though most often used to image work-function variations of conductive surfaces, it can also be used to probe the surface charge on insulating surfaces. In both cases, relating the measured potential to the underlying signal is non-trivial. Here, general relationships are derived between the measured SKPM voltage and the underlying source, revealing either can be cast as a convolution with an appropriately scaled point spread function (PSF). For charge that exists on a thin insulating layer above a conductor, the PSF has the same shape as what would occur from a work-function variation alone, differing by a simple scaling factor. This relationship is confirmed by: (1) backing it out from finite-element simulations of work-function and charge signals, and (2) experimentally comparing the measured PSF from a small work-function target to that from a small charge spot. This scaling factor is further validated by comparing SKPM charge measurements with Faraday cup measurements for highly charged samples from contact-charging experiments. These results highlight a heretofore unappreciated connection between SKPM voltage and charge signals, offering a rigorous recipe to extract either from experimental data.

1. Introduction

Quantitative measurement of surface charge is important toward understanding processes ranging from contact charging and electrostatic discharge to lubrication and adsorption.[1–4] In turn, these processes find applications in realms as diverse as industrial manufacturing, fabrication of nano-materials, or even cell adhesion.[5–8] Scanning Kelvin probe microscopy (SKPM), is a technique for measuring the electrostatic potential near surfaces,[9–11] and, although most often used to measure work functions or contact potential differences of conducting surfaces,[12,13] it can also give information about the surface and bulk charge density of insulating samples.[14,15] As with similar techniques, including Kelvin Probe Force Microscopy (KPFM), the measured signal is an amalgamation of multiple contributions – including work function, charge, and geometry – complicating the process of extracting the underlying charge signal.

A key difficulty in using SKPM, on charged surfaces is the quantitative conversion of the measured potential (with units of volts) into surface charge density (with units of coulombs per square meter). **Figure 1** illustrates the problem; the SKPM signal is related to the current induced in a probe as it is vibrated above a sample, which in turn depends on the electrostatic interaction between the probe/sample, the system geometry, and the electrostatic properties of the sample/medium. To recover an estimate for the surface charge, one must account for distortions in the measured surface potential caused by the geometry, as well as convert from units of potential to units of charge density. While the electrostatic field profile due to a charge on a surface, and the connection between measured potential and charge is somewhat understood from a theoretical point of view,[16,17] the conversion from measured potential back to charge remains challenging. One widely used heuristic is to assume a capacitor-like relationship between charge and measured potential, i.e., $\sigma = \frac{\delta}{\epsilon} V_S$, where σ is surface charge density, δ is the insulator thickness, ϵ is its permittivity and V_S is the measured voltage.[18–21] This expression is sufficient to give the correct units for charge. Though it is widely used, we have never seen a rigorous derivation of it. Another shortcoming is that it does not account for the system geometry, i.e., the fact that the shape of the probe, its distance to the surface, and the thickness of the surface all "smear out" the underlying source. Moreover, it is not clear when it is applicable. How thick can the insulator be before it fails? How large can ϵ be? Hence, at present using this "capacitor heuristic" – where the charge is assumed to be proportional to the measured potential – is at best an educated guess, as it lacks a rigorous framework to back it up.

In this work, we focus on rigorously understanding the connection between signals from surface charge (SQ) and work function differences (WF) in SKPM. We begin by deriving a relationship between the measured signal, SQ and WF. Both the signals from WF and SQ contribute cumulatively to the total measured

I. C.D. Lenton, F. Pertl, L. Shafeek, S. R. Waitukaitis
Institute of Science and Technology Austria
Am Campus 1, Klosterneuburg 3400, Austria
E-mail: isaac.lenton@manchester.ac.uk

The ORCID identification number(s) for the author(s) of this article can be found under https://doi.org/10.1002/admi.202500521

DOI: 10.1002/admi.202500521

signal: in both cases the measured signal can be formulated as a convolution of the underlying charge/work-function signal and an appropriately scaled point spread function (PSF). We show rigorously that the PSF of a charge pattern on the surface of a thin dielectric above a conductive back electrode has the same shape as the PSF due to work function variations on the back electrode alone (i.e., absent the insulating layer), but indeed differs by the widely presumed scaling factor δ/ϵ. We directly test this by performing finite-element simulations corresponding to the two situations, which demonstrates how it fails if the insulator is too thick or the permittivity too high. We further test it by comparing experimental measurements of both SQ and WF PSFs. Finally, we show how quantitative surface charge measurements can be acquired by using a PSF to deconvolve SKPM data, and validate measurements of total charge by comparing to results from a Faraday cup. While our focus in this work is on SKPM, this general approach could be extended to other Kelvin probe based techniques for measuring surface charge.

2. Theory

SKPM involves scanning a vibrating conductive probe above a surface at a known frequency, and measuring the current induced in the probe due to the local electrostatic field at the same frequency using a lock-in amplifier.[9–11] By additionally applying a DC voltage between the probe and the sample (or for thin insulating samples, a backing electrode below the sample) and using feedback, the lock-in current in the probe can be minimised. The SKPM potential image (Figure 1b) corresponds to this voltage that minimises the lock-in current signal at different locations above the sample. In order to extract the surface charge (Figure 1c), we need to account for all the factors which can contribute to the measured signal, such as system geometry, long-range electrostatic interactions between the probe and sample, and properties of the insulating layer.

For the geometry shown in Figure 1a, consisting of a thin homogeneous insulating layer above a conducting surface, we can take a first-principles approach to deriving the relationship between measured potential and the underlying source. Effectively, SKPM involves finding

$$0 = i(t) \equiv \frac{dQ}{dt} \tag{1}$$

where $i(t)$ is the current measured by the lock-in amplifier and $Q(t)$ is the charge in the SKPM probe as a function of time t. Given the timescale of the probe oscillations is slow (~50 Hz), we can assume the system is electrostatic, and hence the charge distribution can be expressed as a surface integral involving the scalar potential ϕ on the probe surface, $\mathcal{S}_T$:

$$Q = -\epsilon_0 \oint_{\mathcal{S}_T} \nabla_x \phi(x) \cdot dn_x \tag{2}$$

where ϵ_0 is the vacuum permittivity, ∇_x denotes the gradient operator with respect to the spatial coordinate $x \in \mathbb{R}^3$, and dn_x is a unit area element pointing normal to the surface. If we consider

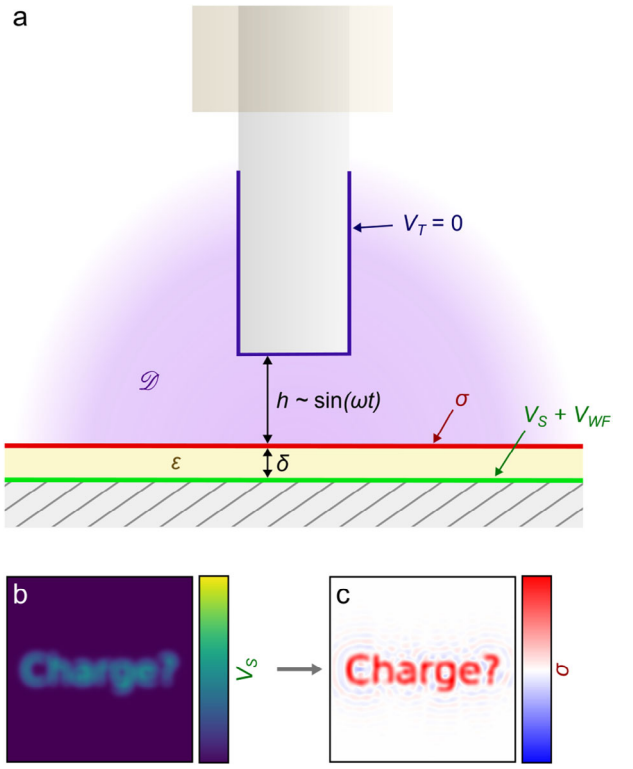

Figure 1. Depiction of surface charge measurement with SKPM. a) The probe-sample system forms a capacitor. When the probe is vibrated, the measured current depends on the geometry and properties of the system (the relevant parameters are discussed further in Section 2). b,c) Converting the measured potential (b) into an estimate for the surface potential (c) requires accounting for the complexity of this system.

a small time-dependent movement of the tip, dh, we can rewrite Equation (1) as:

$$0 = \frac{dh}{dt}\frac{dQ}{dh} = \oint_{\mathcal{S}_T} \frac{d}{dh} \nabla_x \phi(x) \cdot dn_x \tag{3}$$

For an arbitrary domain, $\mathcal{D}$, bounded by a surface $\mathcal{S}$, we can write the electrostatic potential in terms of a Green's function, $G(x, \xi)$ for $(x, \xi) \in \mathbb{R}^3$,

$$\phi(x) = \frac{1}{4\pi\epsilon_0} \int_D \rho(\xi) G(x, \xi)\, d\xi + \frac{1}{4\pi} \oint_S V_S \nabla_\xi G(x, \xi) \cdot dn_\xi \tag{4}$$

where ρ describes point sources (i.e., charges) within the domain and V_S describes the potential on the boundaries. The Green's function accounts for effects from system geometry (i.e., the shape of the probe, the insulating layer, and the probe location relative to the surface), and V_S describes the potential on the boundaries. We note that $G(x, \xi)$ vanishes at the boundaries ($\xi \in \mathcal{S}$). For the system shown in Figure 1, choosing the tip potential as zero ($V_T = 0$), and the potential far from the sample as zero ($V_{\xi \to \infty} = 0$), leaves the only non-zero V_S terms corresponding to the integral over the sample surface (i.e., the combination

of applied potential V_S and the potential arising due to surface work function variations V_{WF}: $V_S + V_{WF} \neq 0$). In practice, what is typically measured is the contact potential difference between the probe and sample rather than a direct measurement of the work function. These contact potential difference measurements can be converted to work function measurements after calibration against a suitable calibration target.[22,23]

If we limit our attention to a 2D sample with a 2D surface charge distribution, $\sigma(\xi)$, on some plane, S_σ, above but parallel to the lower boundary, S_Φ, the potential simplifies to two surface integrals

$$\phi(x) = \frac{1}{4\pi\epsilon_0}\oint_{S_\sigma}\sigma(\xi)G(x,\xi)\,d\xi + \frac{1}{4\pi}\oint_{S_\Phi}(V_{\mathrm{WF}}(\xi)-V_S)\nabla_\xi G(x,\xi)\cdot dn_\xi \tag{5}$$

Substituting this expression for the potential into Equation (3) gives

$$0 = \oint_{S_T}\frac{d}{dh}\nabla_x\left(\frac{1}{\epsilon_0}\oint_{S_\sigma}\sigma(\xi)G(x,\xi)\,d\xi + \oint_{S_\Phi}(V_{\mathrm{WF}}(\xi)-V_S)\nabla_\xi G(x,\xi)\cdot dn_\xi\right)\cdot dn_x \tag{6}$$

By noting that the scalar potential is finite, we can re-arrange for the applied surface voltage V_S:

$$V_S\oint\nabla_\xi U(\xi)\cdot dn_\xi = \frac{1}{\epsilon_0}\oint\sigma(\xi)U(\xi)\,d\xi + \oint V_{\mathrm{WF}}(\xi)\nabla_\xi U(\xi)\cdot dn_\xi \tag{7}$$

where we have dropped the domains in the above surface integrals as they are implied by the integrand, and we have introduced

$$U(\xi) = \oint_{S_T}\frac{d}{dh}\nabla_x G(x,\xi)\cdot dn_x \tag{8}$$

To convert the above expression for the voltage at a single point into a potential map describing the surface charge or contact potential difference, we first consider how the Green's function changes when the tip is translated. For an infinitely wide uniform/flat sample, the Greens's function is translationally invariant, i.e., $G(x, \xi - \eta) = G(x, \xi)$. Substituting $\xi \to \eta - \xi$ into the above, we can write the voltage distribution $V(\eta)$ for a scan over the surface as:

$$V_S(\eta) = \oint\frac{u_0(\xi)}{u_2(\eta)}\sigma(\eta-\xi)\,d_\xi + \oint\frac{u_1(\xi)}{u_2(\eta)}V_{\mathrm{WF}}(\eta-\xi)\,d_\xi \tag{9}$$

where we have introduced

$$u_0(\eta) \equiv \frac{1}{\epsilon_0}U(\eta),$$
$$u_1(\eta) \equiv \nabla U(\eta)\cdot n, \tag{10}$$
$$u_2(\eta) \equiv \oint\nabla U(\eta)\cdot dn$$

The factors $P_\sigma = \frac{u_0}{u_2}$ and $P_{\mathrm{WF}} = \frac{u_1}{u_2}$ correspond to the PSFs for charge and work function in this geometry.

Calculating either of these PSFs analytically from first principles is difficult. As we will show, however, both PSFs can be calculated in finite-element simulations and measured experimentally. One interesting outcome we can see analytically is the relationship between u_0 and u_1. If we determine either of these, we can easily calculate the other by simply integrating or taking the derivative. Furthermore, because in typical SKPM operation the distance between the probe and the sample is large compared to the thickness of the insulating layer (δ), we can use a first-order approximation for the derivative to give

$$u_0(\eta; z=\delta) \approx \frac{\delta}{\epsilon_0}u_1(\eta; z=0) \tag{11}$$

since $u_0(z = 0) = 0$ from the definition of our Green's function (i.e., the requirement that the Green's function vanish at the boundaries). Replacing the vacuum permittivity by the material permittivity ϵ for the region between the charge surface and backing electrode, we recover the simple capacitor relationship between the measured SKPM potential and charge density[19,24]

$$P_\sigma \approx \frac{\delta}{\epsilon}P_{\mathrm{WF}}. \tag{12}$$

As we mentioned in the introduction, this "capacitor heuristic" is widely presumed throughout the literature, but to the best of our knowledge has not been derived. Moreover, our analysis here shows that the relationship is deeper than simple proportionality of surface charge density and voltage. This is because it is not a priori clear that the PSFs in the two cases should be the same; yet they are. This equivalence has significant implications for calibration and measurement with SKPM: it suggests that measuring either the surface charge or work function PSF can give us complete information about the other.

3. Results and Discussion

3.1. Numerical Determination of PSF Shapes

As a first verification of the predictions from the previous section, and to explore over which length and permittivity scales they are valid Equation (12), we built a COMSOL model for our probe-sample system (full details are given in Section 5). **Figure 2**a–c shows the electric potential between the a probe and the surface

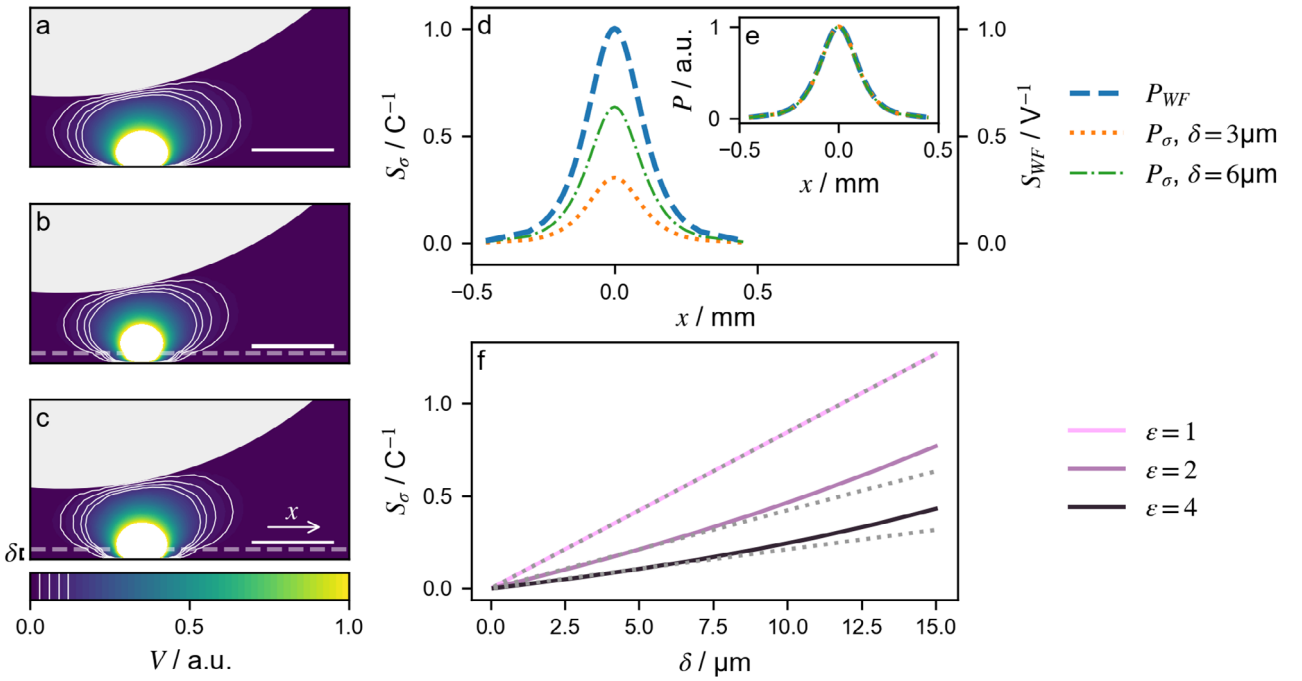

Figure 2. Simulations showing the potential distribution from charge and work function point-like sources and the corresponding PSFs. a–c) Normalised potential distributions between the probe (top hemisphere) and surface (bottom edge) for (a) work function point with no insulator, b) charge point on insulator, and (c) work function point beneath insulator. Scale bar shows 50 μm. The dashed line marks the boundary of the insulator. Contours (white lines) are equally spaced, illustrating the similarity in the potential gradient near the probe surface. d) Simulated PSFs for surface work function (S_{WF}) and charge (S_σ) points at two different heights above the surface e) PSFs in normalised units (P), emphasising the similarity in shape between simulated PSFs S_{WF} and S_σ. f) PSF amplitude as a function of layer thickness (δ) for different permittivities (ϵ). For small insulating layer thicknesses (i.e., small compared to the tip-sample distance and tip diameter), the relationship between signals from work function variations and charge are linear, as illustrated by the dashed lines.

for the three relevant cases: a point-like potential with no insulating layer, a point-charge on an insulating layer, and a point-like potential beneath an insulating layer. These cases are for a relatively thick ($\delta = 6$ μm) insulating layer with a relatively high permittivity ($\epsilon/\epsilon_0 = 4$). The probe position and diameter are comparable to a realistic SKPM measurement with diameter 500 μm and probe-to-surface distance of 60 μm. Near the point-source, the shape of the potential differs significantly, demonstrating how in general $G_\varepsilon \neq G_{\varepsilon_0}$. However, far from the point-source near the probe surface, we can see that the resulting electric field is quite similar for the three cases, supporting the applicability of Equation (12).

Accordingly, the behavior we predict occurs in the simulated PSFs (Figure 2d): all three PSFs have similar shapes, despite corresponding to slightly different physical situations. When the simulated PSFs are normalised by the peak value (Figure 2e), we see this more clearly as they collapse to the same curve. Figure 2f plots the ratio between the work function PSF and the charge density PSF. The linear relationship given by Equation (12) is valid at small δ (relative to the tip-sample distance and tip diameter) for all ϵ, but the range of this becomes shorter with increasing ϵ. Hence, we can conclude that the "capacitor heuristic" is valid for typical insulators (e.g., those with permittivities $\epsilon/\epsilon_0 \lesssim 5$) and typical probe geometries (i.e., large probe-to-sample distance compared to the insulator thickness). For substantially thicker surfaces or higher permittivities, it can indeed be expected to fail miserably.

3.2. Experimental Comparison of PSF Shapes

Beyond simulations, we can validate our ideas experimentally. We do this by fabricating PSF "calibration targets", i.e., very small source features with which we can scan our SKPM to effectively obtain PSFs. These are a small disc of metal and a point-like charge spot for the WF and SQ cases, respectively. For the metal disc, we performed lift-off lithography to evaporate a small gold disc on a silicon wafer and then deconvolved the measured signal by the disc shape to estimate the PSF.[11] For the charge target, we deposited a localized spot (2 μm diameter) of charge on a wafer with a thermally grown SiO_2 layer (thickness $\delta = 3$ μm) using a plasma focused ion beam (PFIB). We confirmed that the surface geometry wasn't changed significantly as a result of the PFIB process by imaging identically prepared samples with atomic force microscopy. Full details are provided in Section 5.

To acquire accurate estimation of the PSF using these charge targets requires a relatively high scan speed to allow complete aquisition before the magnitude of the charge changes significantly.[25] Unlike the numerical PSF, the experimental PSFs account for the effect of the different scan parameters, possible variations in probe shape, including scan speed and tip motion.[11]

SKPM scans for the two cases are shown in **Figure 3**. We confirm again that both PSFs have essentially the same shape; normalizing each by the peak value, they largely collapse on top of each other. The one notable difference is the relative size of the

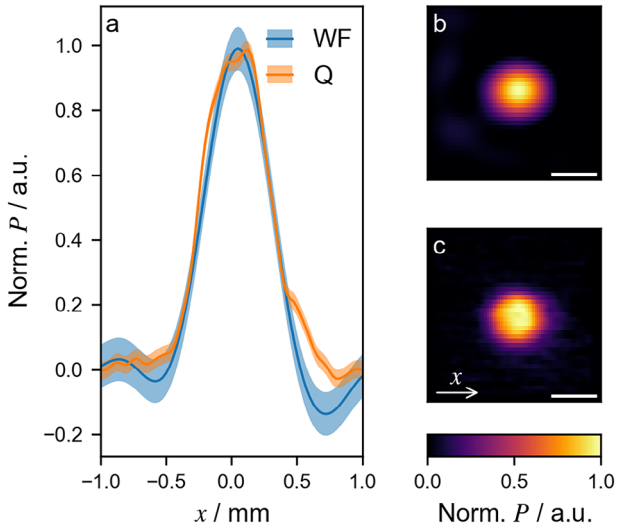

Figure 3. Experimentally measured PSFs for a work function (WF) and charge (Q) signal. a) Comparison between slices of the PSF calculated using the charge target and work function target. Shaded regions show 2σ uncertainty estimate based on the measurement signal-to-noise ratio. b) The estimated PSF for a work function target. c) The estimated PSF for a charge target. Scale bars indicate 500 µm.

error bars. The charge spot produced a significantly larger SKPM signal, much larger than the SKPM system noise. The stronger charge signal also allows measurement of higher frequency parts of the PSF signal, revealing broadening of the PSF near the peak, as we saw in our previous work with slower scan PSFs.[11] The strong negative region in the WF signal around $x = 0.5$ is likely an artifact resulting from a combination of the weak signal and absence of high frequency information. In the Supporting Information, we show the power spectra for these signals, which more clearly demonstrate the improved signal-to-noise achievable with the charge target. Hence, once again we see that our main result is validated.

3.3. Surface Charge Measurement With SKPM

To measure the surface charge with SKPM, we need to separate the contributions from the material/geometry from the contributions due to surface charge and then convert the potential into charge. For a relative charge measurement, e.g., charge added due to a contact with another material, we can simply scan the surface before and after the charging event and compare the potentials

$$V_{s,rel} = V_{s,2} - V_{s,1} = \oint \frac{u_0}{u_2}(\sigma_2 - \sigma_1) \tag{13}$$

where $\sigma_{1,2}$ are the surface charge densities before/after the charging event and the surface integral corresponds to the first term in Equation (9). To estimate the relative charge, we can deconvolve the measured potential by the relevant PSF[11]

$$\sigma = P_\sigma^{-1} \otimes V_{s,rel} \tag{14}$$

where we have used $P_\sigma^{-1}\otimes$ to denote the deconvolution. By using an experimentally measured PSF here, we implicitly account for several measurement specific factors including probe-sample separation, shape of the probe, and stray capacitance between the measurement system. Care is taken to perform measurements only near the centre of the wafer substrate to avoid edge-effects from the finite nature of our samples. This approach is sufficient for many types of contact charging experiments.

Figure 4 depicts a typical contact charging experiment: a sample of PDMS is contacted with a silicon wafer with a thin insulating layer of SiO_2 (thickness δ = 3 µm). After removing the PDMS the surface becomes charged.[8,26,27] Figure 4b shows the relative change in potential before/after the contact event. By deconvolving the signal by the PSF, we recover the surface charge left by the charging event (Figure 4c). We see that the charging is non-uniform, largely due to the pattern we used to cure the PDMS (our institute logo), and partially due to the peeling direction when removing the PDMS stamp, as has been previously described.[8,28] One region acquired a significant positive charge, indicated by the pink region in Figure 4**c** where we were unable to measure the charge accurately due to the limited voltage range of our SKPM. The resolution of the recovered charge image is related to the measurement bandwidth: a product of the probe size and scan speed; while the accuracy is limited by the measurement noise.

As further validation for the scaling factor used to convert the work function PSF into a charge PSF, we compared SKPM-derived charge measurements to those made with an independent charge-measurement technique. We placed a silicon wafer with a silicon dioxide layer inside a Faraday cup, contacted the wafer with a PDMS stamp and measured the total charge remaining on the wafer after the PDMS was removed from the Faraday cup. We then transferred the wafer to the SKPM, measured the surface charge density and integrated to calculate the net charge.

The results (**Figure 5**) show good agreement, especially in

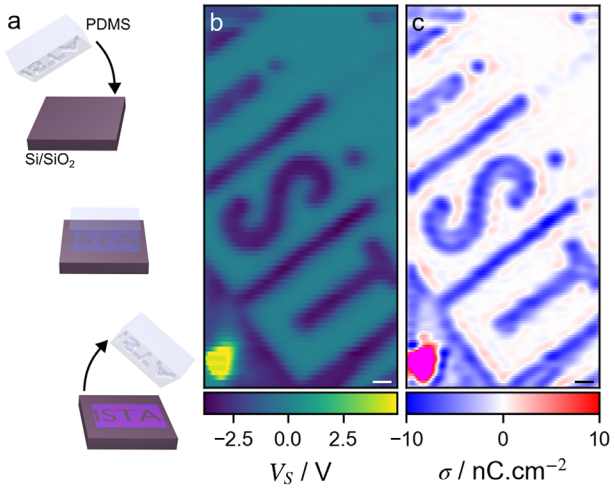

Figure 4. Example SKPM potential measurement and the deconvolution to give the surface charge density. a) A charge pattern is created by pressing a PDMS stamp against a silicon wafer with a thin oxide layer. b) The resulting SKPM signal b) can be deconvolved with the PSF to give the surface charge density c). Scale bars show 1 mm.

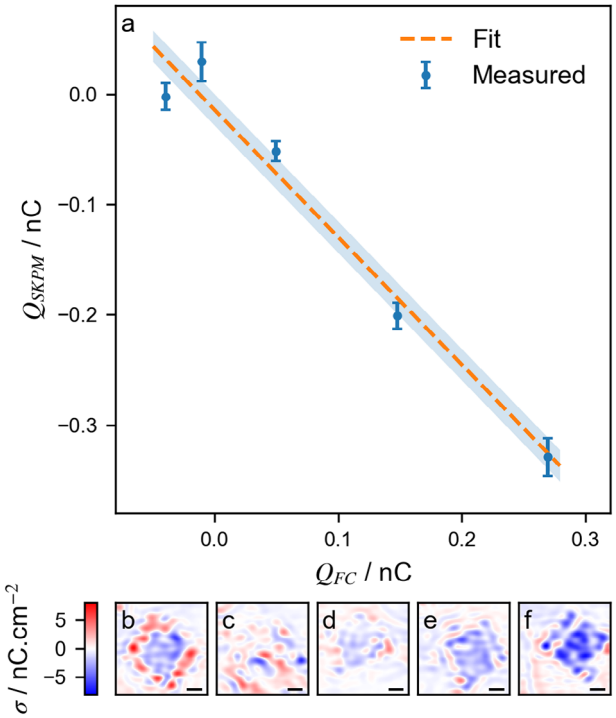

Figure 5. Comparison between SKPM and Faraday cup charge measurements. a) Plot showing SKPM Q_{SKPM} and Faraday Cup Q_{FC} charge measurements. Panel b–f) shows the SKPM scans for samples in order of increasing charge for each data point in the plot. Scale bars show 1 mm. Error bars show 1σ uncertainty in SKPM measurement (see Section 5 for details), FC instrument measurement uncertainty was typically better than 1% and error bars are omitted. Shaded region shows uncertainty in fit.

the correlation factor: –1.15 ± 0.14 C/C. The sign difference corresponds to a difference in convention used by the electrometer and SKPM. The main sources of error, including the DC shift, was estimation of the background charge level, including how much charge was already on the surface before contact, and charge transferred to the sample during handling. For relative charge measurements, we find that the accuracy is comparable to the Faraday cup charge estimation (for these samples). Other factors contributing to the difference in slope may be related to variations in oxide layer thickness, variations in permittivity, or the limitations of the simple capacitor-like approximation we used for the PSFs.

4. Conclusion and Perspectives

We have derived a relationship between the PSFs for work function and surface charge density in SKPM, and validated it in both in simulations and experimentally. We found that, at least for thin insulating layers and low dielectric constants, the widely-presumed capacitor scaling is valid. However, we furthermore have shown that the PSFs necessary to deconvolve SKPM data for the charge/potential case have the same shape, differing only by the capacitive scaling factor. While we have focused on the macroscopic SKPM technique, our results should also be extendable to the nanoscopic counterpart of Kelvin Probe Force Microscopy (KPFM), although the differences in length scales may limit the applicability. Our focus was on the connection between surface charge and work function on a planar surface; however, we believe these results could be extended to other geometries and bulk charge distributions.[17] Furthermore, we validated that SKPM is a suitable tool for quantitative measurement of surface charge on thin insulating materials. Importantly, measurements can be calibrated without requiring separate simulations or calibrations for the individual charge or work function cases. This has two important consequences; first, it enables the fabrication of calibration targets with much higher signals compared to conventional work function-based targets, overcoming problems we previously identified with the fabrication of calibration targets for SKPM,[11] and second, it removes the need for repeated calibration of different insulation-thickness combinations. We believe these results could be useful for understanding phenomena as diverse as contact electrification, corrosion, and formation of bio-films.[25,29,30]

5. Experimental Section

Numerical Modeling: To simulate the work function and charge density PSFs were created, a electrostatics model in COMSOL Multiphysics 5.3a. For calculating the work function PSFs, a small potential disc was positioned on a grounded plate at different positions bellow the SKPM probe. To explore the effect of adding a thin insulating layer, this simulation was repeated with a thin dielectric layer covering the disc plate. For calculating the charge PSFs, a dielectric layer was added above the plate and added a point charge on the interface between the dielectric layer and air. To calculate the SKPM potential, the current density was compared in the probe at two different heights, as it was described in the earlier work.[11]

Silicon Dioxide Wafer Preparation: Silicon dioxide wafer pieces with varying oxide thicknesses were prepared by first cleaning using a two step solvent clean (Acetone and Isopropyl alcohol in an ultrasonic bath) and then baking at grater than 120°C (typically 300°C) for more than 30 min. Different cleaning conditions give different initial surface potentials. It was found that the baking step was important for achieving a uniform initial charge distribution.

PFIB Target Fabrication: To fabricate the point-like charge target, a Helios G4 PFIB UXe was used with e-beam and ion-beam to create a small charge spot on a silicon dioxide wafer. Clean 3 µm oxide wafers were mounted on SEM pin stubs using double sided carbon tape. Samples were loaded into the PFIB and the system was pumped to vacuum. After waking the e-beam and ion-beam, we positioned the e-beam and ion-beam at the corner of the wafer in order to link the stage and orientate the sample. The ion-beam was set to 10 pA current and 30 kV acceleration voltage. Both the ion- and e-beam imaging were then stopped, this was important to prevent unwanted charging of the sample due to scanning of the beams in imaging mode. The sample was then orientated perpendicular to the ion-beam and positioned so the ion beam was focused directly above the desired target location. The ion-beam was configured to write a circular pattern using the default milling parameters for Si. It was found that writing a circle with diameter 2 µm, with dosage per exposure of 1.0×10^{-11} pC/µm^2 and 1 µs dwell time produced a target that could be measured without saturating the SKPM. Total exposure time was approximately 4 s with an accumulated dosage of approximately 7 pC/µm^2 (total dosage of approximately 21 pC). The system was then shutdown, the chamber vented and the sample removed. The sample was transferred immediately to the SKPM where argon was used to reduce the humidity above the sample in order to reduce charge decay.[31]

PDMS Stamp Fabrication: For creating charge patterns, PDMS stamps were fabricated using a traditional soft-lithography approach. New silicon wafers (p-type, Boron, ⟨100⟩, polished) were cleaned using isopropanol in an ultrasonic bath for 2 min, dried with nitrogen, and baked at 110° C for 2 min to remove any residual water or isopropanol. SU-8 (GM1075, Engineering Solutions) was spin coated on the wafer at 500 rpm

for 15 s to spread the SU-8 and then 100 s at 950 rpm to achieve the desired thickness (~200 µm). The wafer was baked for 10 min at 120° C. The wafer was loaded into the mask aligner (EVG 610 with mercury bulb light source, EV Group) and exposed to 750 mJ/cm^2 with the target pattern. Patterns were designed using Creo Parametric and printed on 0.18 mm Polyethylene terephthalate (PET) film (JD PhotoData). The mask was mounted on a 1.5 mm glass plate to more easily load it into the mask aligner.

Post-exposure, the wafer was baked at 95° C for 1 h and then developed in SU-8 developer with mild agitation, before being rinsed with isopropanol and hard baked for 5 min at 135° C. To allow easy removal of the PDMS stamp from the SU-8 stamp, the wafer was dry silinised: samples to be silinised were placed in a vacuum desiccator with a small quantity of silane (448931-10G, Sigma-Aldrich), pressure was reduced, vacuum turned off, and left for 2-3 hours. For the PDMS stamps, 50 g of PDMS (SYLGARD 184, Dow Chemical Company) was prepared with a 10:1 ratio (50 g is sufficient to cover three 100 mm wafers). PDMS was poured over the SU-8 stamps and degassed using a vacuum desiccator and nitrogen gun to remove any bubbles before curing in an oven for 4 h at 80° C. PDMS stamps could then be removed from the wafer when required.

Faraday cup Charge Measurements: To verify the SKPM charge measurement, 10 × 10 mm Si wafer pieces with 3 µm thermally grown oxide were cleaned, discharged, and mounted in a custom made Faraday cup connected to an electrometer (B2987B, Keysight). Prior to measurement, the electrometer was self-calibrated according to the manual and left for approximately 1 hour to allow it to stabilise. The Faraday cup was purged with clean dry air prior to loading each sample, excess humidity in the Faraday cup would often cause large drifts in the electrometer signal. The electrometer was zeroed and a piece of PDMS (approximately 3 × 3 mm) attached to a wooden stick was contacted with the wafer sample. The electrometer value was recorded after the PDMS piece was removed from the Faraday cup. After contact, samples were transferred to the SKPM to be scanned. Care was taken to avoid touching the sample surface after contact, potentially altering the charge – however, there may still be some additional contribution to the measurement uncertainty due to the handling and transport of the samples from the Faraday cup to the SKPM.

SKPM Charge Estimation: The wafer was scanned with SKPM and integrated the surface charge density to give the net charge. Due to how the sample was mounted, it is difficult to scan the whole wafer, so only the central region around where the PDMS was contacted with the wafer was scanned. To estimate the error, the standard deviation was calculated along the edge of the scanned region to give an estimate for the variation in background signal across the wafer.

Supporting Information

Supporting Information is available from the Wiley Online Library or from the author.

Acknowledgements

This project received funding from the European Research Council (ERC) under the European Union's Horizon 2020 research and innovation programme (Grant agreement No. 949120). This research was supported by the Scientific Service Units of The Institute of Science and Technology Austria (ISTA) through resources provided by the Miba Machine Shop, Nanofabrication Facility, Scientific Computing Facility, and Lab Support Facility. The authors wish to thank Dmytro Rak and Juan Carlos Sobarzo for letting us use their equipment. The authors wish to thank Evgeniia Volobueva for advice in preparing PFIB samples. The authors wish to thank the contributions of the whole Waitukaitis group for useful discussions and feedback.

Conflict of Interest

The authors declare no conflict of interest.

Author Contributions

I.L. was responsible for conceptualization, formal analysis, conducting simulations and investigations, as well as drafting the original manuscript. F.P. contributed to the investigation and provided essential resources. L.S. also supported the project by providing resources. S.W. supervised the work, secured funding, and contributed to reviewing and editing the manuscript.

Data Availability Statement

The data that support the findings of this study are available from the corresponding author upon reasonable request.

Keywords

contact charge, point charge, point spread function, scanning Kelvin probe microscopy, surface charge

Received: June 8, 2025
Revised: August 8, 2025
Published online: August 29, 2025

[1] D. J. Lacks, T. Shinbrot, *Nat. Rev. Chem.* **2019**, *3*, 465.
[2] A. Kumada, Y. Shimizu, M. Chiba, K. Hidaka, *J. Electrostat.* **2003**, *58*, 45.
[3] S. Li, P. Bista, S. A. L. Weber, M. Kappl, H.-J. Butt, *Langmuir* **2022**, *38*, 12610.
[4] Y. Fang, C. K. Ao, Y. Jiang, Y. Sun, L. Chen, S. Soh, *Nat. Commun.* **2024**, *15*, 1.
[5] J. Méndez Harper, C. S. McDonald, E. J. Rheingold, L. C. Wehn, R. E. Bumbaugh, E. J. Cope, L. E. Lindberg, J. Pham, Y.-H. Kim, J. Dufek, C. H. Hendon, *Matter* **2024**, *7*, 266.
[6] T. Hackl, G. Schitter, P. Mesquida, *ACS Nano* **2022**, *16*, 17982.
[7] S. Metwally, U. Stachewicz, *Mater. Sci. Eng., C* **2019**, *104*, 109883.
[8] Y. I. Sobolev, W. Adamkiewicz, M. Siek, B. A. Grzybowski, *Nat. Phys.* **2022**, *18*, 1347.
[9] W. A. Zisman, *Rev. Sci. Instrum.* **1932**, *3*, 367.
[10] P. P. Craig, V. Radeka, *Rev. Sci. Instrum.* **1970**, *41*, 258.
[11] I. C. D. Lenton, F. Pertl, L. Shafeek, S. R. Waitukaitis, *arXiv* **2024**, https://doi.org/10.1063/5.0215151.
[12] A. Nazarov, M.-G. Olivier, D. Thierry, *Progress in Organic Coatings* **2012**, *74*, 356.
[13] A. Nazarov, D. Thierry, *Front. Mater.* **2019**, *6*, 462587.
[14] M. Nalbach, H. Kliem, *Phys. Status Solidi A* **2000**, *178*, 715.
[15] B. Martin, H. Kliem, *IEEE Trans. Dielectr. Electr. Insul.* **2008**, *15*, 560.
[16] A. Sadeghi, A. Baratoff, S. Goedecker, *Phys. Rev. B* **2013**, *88*, 035436.
[17] A. M. Somoza, E. Palacios-Lidón, *Phys. Rev. B* **2020**, *101*, 075432.
[18] D. Heile, R. Olbrich, M. Reichling, P. Rahe, *Phys. Rev. B* **2023**, *108*, 085420.
[19] W. Cai, N. Yao, *Sci. Rep.* **2016**, *6*, 1.
[20] A. M. Barnes, A. D. Dinsmore, *J. Electrostat.* **2016**, *81*, 76.
[21] E. Palleau, L. Ressier, Ł. Borowik, T. Mélin, *Nanotechnology* **2010**, *21*, 225706.
[22] W. N. Hansen, G. J. Hansen, *Surf. Sci.* **2001**, *481*, 172.
[23] P. A. Fernández Garrillo, B. Grévin, N. Chevalier, Ł. Borowik, *Rev. Sci. Instrum.* **2018**, *89*, 4.
[24] L. Bürgi, T. Richards, M. Chiesa, R. H. Friend, H. Sirringhaus, *Synth. Met.* **2004**, *146*, 297.
[25] F. Pertl, I. C. D. Lenton, T. Cramer, S. Waitukaitis, *arXiv* https://doi.org/10.1103/lcsm-xxty.

[26] H. T. Baytekin, A. Z. Patashinski, M. Branicki, B. Baytekin, S. Soh, B. A. Grzybowski, *Science* **2011**, *333*, 308.
[27] F. Pertl, J. C. Sobarzo, L. Shafeek, T. Cramer, S. Waitukaitis, *Phys. Rev. Mater.* **2022**, *6*, 125605.
[28] M. P. Reiter, T. Shinbrot, *Tribology Lubrication Technology* **2021**, 24.
[29] H. Zhu, R. Ramprasad, *Phys. Rev. B* **2011**, *83*, 081416.
[30] E. Rahimi, A. Imani, M. Lekka, F. Andreatta, Y. Gonzalez-Garcia, J. M. C. Mol, E. Asselin, L. Fedrizzi, *38*, 10854.
[31] M. Navarro-Rodriguez, E. Palacios-Lidon, A. M. Somoza, *Appl. Surf. Sci.* **2023**, *610*, 155437.